Hindawi
International Journal of Chemical Engineering
Volume 2019, Article ID 3926897, 13 pages
https://doi.org/10.1155/2019/3926897

Research Article

A Moving Boundary Model for Isothermal Drying and Shrinkage of Chayote Discoid Samples: Comparison between the Fully Analytical and the Shortcut Numerical Approaches

Alessandra Adrover[1] **and Antonio Brasiello**[2]

[1]*Dipartimento di Ingegneria Chimica Materiali e Ambiente, Università degli Studi di Roma "La Sapienza", via Eudossiana 18, 00184 Roma, Italy*
[2]*Dipartimento di Ingegneria Industriale, Università degli Studi di Salerno, via Giovanni Paolo II, 132 84084 Fisciano, Salerno, Italy*

Correspondence should be addressed to Alessandra Adrover; alessandra.adrover@uniroma1.it

Received 30 November 2018; Accepted 13 March 2019; Published 16 May 2019

Academic Editor: Xunli Zhang

A moving boundary model for food isothermal drying and shrinkage is applied to predict the time decay of water content and sample volume, as well as water diffusivity for chayote discoid slices in the temperature range 40–70°C. The core of the model is the shrinkage velocity $\mathbf{v}$, assumed equal to the water concentration gradient times a shrinkage function α representing the constitutive equation of the food material under investigation. The aim is to provide a case study to analyze and quantify differences and accuracies of two different approaches for determining the shrinkage function α from typical experimental data of moisture content X/X_0 vs. rescaled volume V/V_0: a fully analytical approach and a shortcut numerical one.

1. Introduction

Mathematical modeling in chemical engineering historically provided the necessary support for understanding physics and transport phenomena that underlie the chemical processes. Mathematical models are also useful tools for the optimization of experimental campaigns and for scale-up from laboratory to industrial scale. During decades, more and more mathematical modeling techniques have been developed [1, 2] bridging different spatial and temporal scales from the microscopic to the macroscopic ones [2, 3] through the mesoscale [4–6]. The translation of chemical processes into equations has always been the unavoidable step for efficient plant design, process analysis, or control.

Food process engineering represents one of the most promising research fields in chemical engineering that could benefit the enhancements of the theoretical research. It was quite intentionally forgotten, in the past, due to the complexity of food materials and of related transformation processes. Among them, drying is undoubtedly one of the most investigated, probably for its huge industrial impact [7–9]. Actually, the drying process is very complex as it implies material transformation at several spatial scales (e.g., porous structure variation and volume changes).

Far from accomplishing a multiscale mathematical formulation able to account for the complexity of the all the phenomena involved [10–12], mathematical models for drying try to capture those features that are more important from the technological point of view. Shrinkage is the most relevant phenomenon connected to drying since it influences consumer quality perception, costs for transportation, and storage [13]. Among the wide literature on this topic, it is worth mentioning some works: [14] in which shrinkage kinetic laws are discussed; [15–17] in which applications of mathematical modeling techniques to food drying can be found; [10] in which a general discussion on advanced computational modeling for drying can be found; [13, 18–20] in which different advanced approaches for linking water content evolution to shrinkage can be found.

In particular, Adrover et al. [21, 22] recently developed a mathematical model with moving boundary for drying of food materials by suitably modifying a classical moving boundary model originally developed in [23, 24] for mass transport, swelling, and dissolution in polymers [25, 26]. The novelty consists in the introduction of a new constitutive equation linking the boundary movement to the water concentration gradient through a proportionality factor α representing the fingerprint of the food material under investigation.

In [21, 22], the authors were able to predict both water content evolution and volume reduction following two different approaches for the determination of the proportionality factor α from experiments: a fully analytical approach and a shortcut one. Reasonably, from a computational point of view, the first one could be more difficult to apply in many cases of practical interest, e.g., for very complex geometries of food samples, while the second one could not be accurate.

In this paper, the comparison between the two approaches is carried out by using literature experimental data [27] on chayote discoid slices. In this case, due to both the regular shape and the aspect ratio of the samples, both approaches can be easily adopted. The aim is to provide a case study to test differences in terms of accuracy of prediction of water content evolution, volume reduction, and other significant physical quantities such as the water diffusivity.

2. Moving Boundary Model for Discoid Samples

We briefly recall the model equations derived in [21, 22].

Let L_r be a characteristic length of the food sample, ϕ the point-wise water volume fraction, ϕ_0 the uniform initial water volume fraction, and D the water diffusivity at the operating temperature.

By introducing the dimensionless space and time variables $\tau = tD/L_r^2$, $\mathbf{x} \longrightarrow \mathbf{x}/L_r$, $V \longrightarrow V/L_r^3$, and $S \longrightarrow S/L_r^2$ and the dimensionless differential operators $\nabla \longrightarrow \nabla/L_r$ and $\nabla\cdot \longrightarrow \nabla/L_r\cdot$, the moving boundary model equations for the normalized water volume fraction $\psi = \phi/\phi_0$ attain the form:

$$\begin{aligned}\frac{\partial \psi}{\partial \tau} &= \nabla \cdot (\nabla\psi - \mathbf{v}\psi)\\ &= \nabla \cdot \left(\nabla\psi\left(1 - \alpha(\psi)\phi_0\psi\right)\right), \quad \mathbf{x} \in V(\tau),\end{aligned} \tag{1}$$

$$-\nabla\psi \cdot \mathbf{n}|_{\mathbf{x}_b} = \mathrm{Bi}_m\left(\psi|_{\mathbf{x}_b} - \psi_{eq}\right), \quad \mathbf{x}_b \in S(\tau), \tag{2}$$

$$\frac{d\mathbf{x}_b}{d\tau} = \mathbf{v}|_{\mathbf{x}_b} = \left[\alpha(\psi)\phi_0\nabla\psi\right]\big|_{\mathbf{x}_b}, \quad \mathbf{x}_b \in S(\tau), \tag{3}$$

$$\begin{aligned}\mathbf{v} &= \alpha(\psi)\phi_0\nabla\psi,\\ \mathrm{Bi}_m &= \frac{h_m L_r}{D} K_{eq}\frac{\rho_{air}}{\rho_s},\end{aligned} \tag{4}$$

$$\begin{aligned}V(0) &= V_0,\\ S(0) &= S_0,\\ \psi(\mathbf{x}, 0) &= 1,\end{aligned} \tag{5}$$

where Bi_m is the mass transfer Biot number, h_m is a mass transfer coefficient, ρ_s is the solid (pulp) density, ρ_{air} is the air density at the operating temperature, K_{eq} is the water partition ratio between the gas and the solid phases $H = K_{eq}(\rho_w/\rho_s)\phi$, H being the absolute air humidity (kg water/kg dry air).

The core of the model is the shrinkage velocity $\mathbf{v}$, proportional to the water concentration gradient times a proportionality function $\alpha(\psi)$ tuning, at each point of the system, the relationship between water flux and volume reduction. The shrinkage velocity $\mathbf{v}$ evaluated at the boundary $S(\tau)$ controls the movement of the boundary itself. The time evolution of the sample boundary, as described by equation (3), is consistent with the classical description of boundary movement induced by the transfer of a diffusing substance across the interface [23, 24, 28]. In point of fact, equation (3) represents a generalization of a classical Stefan condition because it accounts for structural changes of the material during the drying process through the introduction of the shrinkage function $\alpha(\psi)$.

In dealing with a discoid sample (radius R_0, thickness L_0) with $R_0 > L_0$, we choose as a reference length $L_r = L_0$ so that the dimensionless initial domain is $(\rho, \zeta) \in [0, R_0/L_0] \times [-1/2, 1/2]$, R_0/L_0 being the discoid aspect ratio.

For high values of the aspect ratio R_0/L_0, a one-dimensional model can be readily adopted, describing the time evolution of the rescaled water volume fraction $\psi(\zeta, \tau)$ along the axial coordinate (associated with the smallest initial dimension L_0) and the time evolution of the dimensionless sample thickness $\widetilde{L}(\tau) = L(\tau)/L_0$ (uniform along the radial direction):

$$\begin{aligned}\frac{\partial \psi}{\partial \tau} &= \frac{\partial}{\partial \zeta}\left(\frac{\partial \psi}{\partial \zeta}\left(1 - \alpha(\psi)\phi_0\psi\right)\right),\\ \zeta &\in \left(-\frac{\widetilde{L}(\tau)}{2}, \frac{\widetilde{L}(\tau)}{2}\right),\end{aligned} \tag{6}$$

$$-\left.\frac{\partial \psi}{\partial \zeta}\right|_{\zeta=\widetilde{L}/2} = \mathrm{Bi}_m\left(\psi|_{\widetilde{L}/2} - \psi_{eq}\right), \tag{7}$$

$$\left.\frac{\partial \psi}{\partial \zeta}\right|_{\zeta=-\widetilde{L}/2} = \mathrm{Bi}_m\left(\psi|_{-\widetilde{L}/2} - \psi_{eq}\right),$$

or equivalently

$$\left.\frac{\partial \psi}{\partial \zeta}\right|_{\zeta=0} = 0, \tag{8}$$

$$\frac{d(\widetilde{L}/2)}{d\tau} = \alpha(\psi)\phi_0\left.\frac{\partial \psi}{\partial \zeta}\right|_{\widetilde{L}/2}, \quad \widetilde{L}(0) = 1. \tag{9}$$

In this 1-d approach, both radial shrinkage and water flux from the discoid lateral surface are neglected.

3. Estimation of the Shrinkage Factor $\alpha(\psi)$

If we adopt a 1-d model for describing the drying process of a discoid sample, the shrinkage factor $\alpha(\psi)$ can be assumed *a priori* or it can be estimated from the *thickness calibration curve* [29, 30], i.e., from experimental data of rescaled thickness L/L_0 vs. the moisture ratio as follows:

$$\frac{d(X/X_0)}{d\tau} = \frac{1}{\phi_0 \alpha(\psi_P)} \frac{d(L/L_0)}{d\tau} \longrightarrow \alpha(\psi_P) \simeq \frac{1}{\phi_0} \frac{dL/L_0}{dX/X_0}, \tag{10}$$

where $\psi_P = \psi(\mathbf{x}_P)$ is the rescaled water volume fraction evaluated, at each time instant t, in a suitable point $\mathbf{x}_P$, called probe point P, placed on the sample surface and evolving in time together with the surface itself. The moisture ratio (or rescaled moisture content) is defined as $X/X_0 = M_w/M_w^0 = (W - W_d)/(W_0 - W_d)$, where M_w is the amount of water at time t, $M_w^0 = \rho_w V_0 \phi_0$ is the initial amount of water in the sample, W is the sample weight (water + pulp) at time t, and W_d is the dry sample weight. In terms of dimensionless variables the moisture ratio is $X/X_0 = \int_V \psi(\mathbf{x}) dV = \int_{-\tilde{L}/2}^{\tilde{L}/2} \psi(\zeta) d\zeta \; X/X_0$.

In Adrover et al. [21, 22], we have shown that a proper choice of the probe point is a point exhibiting the maximum displacement (shrinkage). In this 1-d problem, since ψ is exclusively a function of ζ, the probe point is necessarily the surface point located at $\zeta_P = \tilde{L}(\tau)/2$ and evolving in time together with sample thickness $\tilde{L}(\tau)$.

From equation (10), it is evident that the thickness calibration curve G and, more specifically, its derivative G' actually furnish an experimentally derived shrinkage factor $\alpha_X(X/X_0)$:

$$\alpha_X = \frac{G'(X/X_0)}{\phi_0}, \qquad \frac{L}{L_0} = G\left(\frac{X}{X_0}\right), \qquad G'\left(\frac{X}{X_0}\right) = \frac{dG}{d(X/X_0)}, \tag{11}$$

that depends on the integral quantity X/X_0 and not on the required probe point concentration ψ_P.

In order to recover $\alpha(\psi_P)$ from $\alpha_X(X/X_0)$, it is necessary to identify a function $g(\psi_P, \mathrm{Bi}_m)$ relating X/X_0 to ψ_P, thus obtaining

$$X/X_0 = g(\psi_P, \mathrm{Bi}_m) \longrightarrow \alpha(\psi_P) = \alpha_X(g(\psi_P, \mathrm{Bi}_m)) = \frac{G'(g(\psi_P, \mathrm{Bi}_m))}{\phi_0}. \tag{12}$$

By considering that ψ_P explores the entire range of values of ψ (from $\psi_P = 1$ at $t = 0$ to $\psi_P = \psi_{eq}$ for $t \longrightarrow \infty$), once $\alpha(\psi_P)$ has been derived, we can adopt the same expression for $\alpha(\psi)$ to evaluate the shrinkage velocity at each point in the domain.

The simplest model that can be adopted for the $g(\psi_P, \mathrm{Bi}_m)$ function is a linear model, i.e., $X/X_0 = \psi_P$ that implies $\alpha(\psi_P) = \alpha_X(\psi_P) = G'(\psi_P)/\phi_0$ on the boundary and consistently

$$\alpha(\psi) = \frac{G'(\psi)}{\phi_0}, \tag{13}$$

at each point in the sample domain.

By observing that

$$\frac{X}{X_0} = \psi_{av}\left(\frac{L}{L_0}\right), \qquad \psi_{av} = \frac{1}{\tilde{L}} \int_{-\tilde{L}/2}^{\tilde{L}/2} \psi(\zeta) d\zeta \geq \psi_P \; \forall t, \quad \forall \mathrm{Bi}_m, \tag{14}$$

it is easy to see that the linear approximation $X/X_0 = \psi_P$ underestimates X/X_0 at short time scales, when $L/L_0 \simeq 1$, while it overestimates X/X_0 at large time scales, when $\psi_{av} \simeq \psi_P$ and $L/L_0 \ll 1$ (Figure 8 in Appendix). However, the linear approximation $g(\psi_P, \mathrm{Bi}_m) = \psi_P$, independent of Bi_m, and the resulting shrinkage function equation (13) represents an acceptable compromise between simplicity and a reasonable physical description of the drying process. Moreover, equation (13) represents a good starting point for a more accurate estimate of the shrinkage factor $\alpha(\psi)$.

In order to derive a more accurate explicit expression for $g(\psi_P, \mathrm{Bi}_m)$, we can adopt two different strategies: (i) a fully analytical approach [21] that can be easily applied for foods characterized by linear of quadratic calibration curves $G(X/X_0)$ and (ii) a shortcut numerical approach [22] that can handle any nonlinear function $G(X/X_0)$.

In order to compare the two different approaches, we focus on experimental data of convective hot-air drying of chayote discoid samples characterized by a high initial aspect ratio $R_0/L_0 > 5$ so that the 1-d model, described above, can be reasonably applied.

4. Chayote Discoid Samples Air-Drying

We analyze experimental data of convective hot-air drying of chayote discoid samples (data from [27]). Fruits were washed and peeled. Cylindrical slices with initial radius $R_0 = 35$ mm and initial thickness $L_0 = 6$ mm were prepared. The discoid aspect ratio is $R_0/L_0 \simeq 5.83$. Chayote drying (at $T = 40$, 50, 60, 70°C) was carried out in a convective dryer with air velocity 2 (m/s). The initial moisture content was 93.38 ± 1.03 g water/100 g product. The initial water volume fraction was $\phi_0 = 0.525$ [31]. Available experimental data are the moisture ratio X/X_0 vs. time (min) and and the thickness calibration curves L/L_0 vs. X/X_0 at the four temperatures analyzed.

In [21, 22], Adrover et al. have shown that low values of Bi_m lead to a smoother and flat boundary profile of the sample, while higher values lead to pronounced cusps. By considering the air velocity in the convective dryer and since no information are reported in [27] regarding significant nonuniformities of the sample thickness along the radial direction, we assume in the further analysis a low value for Bi_m, namely, $\mathrm{Bi}_m \in [1, 2]$.

Figures 1(a) and 1(b) show experimental data for L/L_0 vs. X/X_0 and two different approximating functions, both valid in the entire range of temperature analyzed: a second-order polynomial function $G^{2nd}(X/X_0)$ (Figure 1(a)) and a more accurate fourth-order polynomial function $G^{4th}(X/X_0)$ (Figure 1(b)):

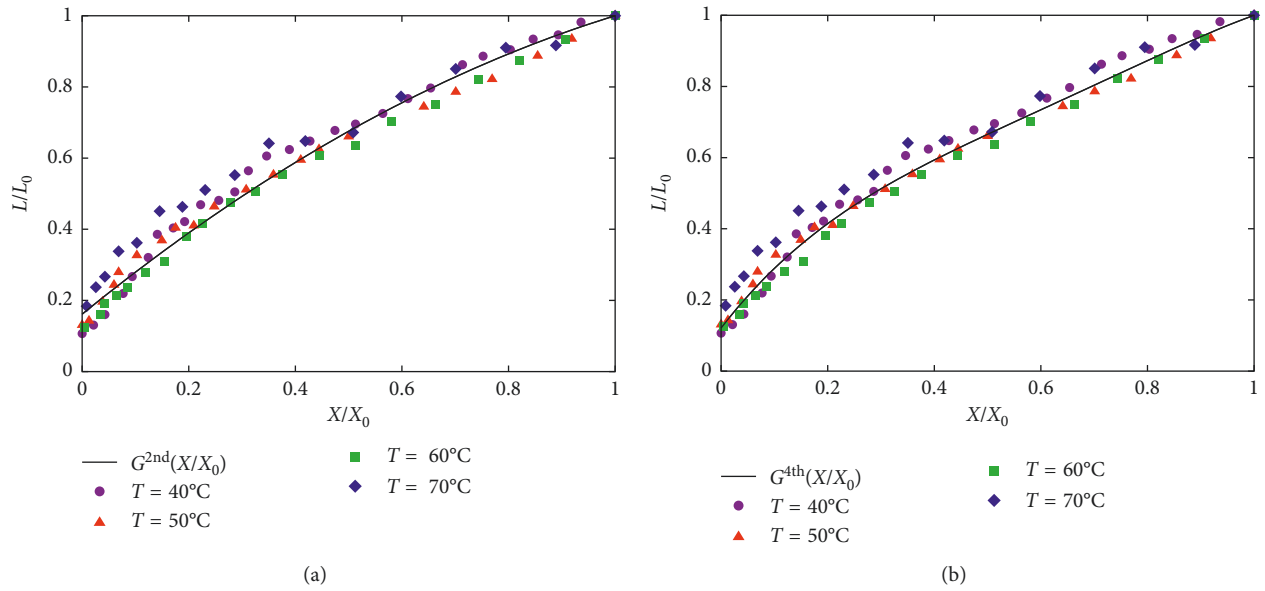

FIGURE 1: Experimental data L/L_0 vs. X/X_0 for chayote discoid samples at four different temperatures $T = 40, 50, 60,$ and 70°C. Least-square best fit with (a) a second-order polynomial function G^{2nd} (equation (15)) and (b) a fourth-order polynomial function G^{4th} (equation (16)).

$$G^{2nd}\left(\frac{X}{X_0}\right) = 1 - \sum_{j=1}^{2} \gamma_j \left(1 - \frac{X}{X_0}\right)^j, \quad \gamma_1 = 0.460, \quad \gamma_2 = 0.378, \tag{15}$$

$$G^{4th}\left(\frac{X}{X_0}\right) = 1 - \sum_{j=1}^{4} \beta_j \left(1 - \frac{X}{X_0}\right)^j, \quad \beta_1 = 0.411, \quad \beta_2 = 1.155, \quad \beta_3 = -2.131, \quad \beta_4 = 1.445. \tag{16}$$

The fourth-order polynomial function $G^{4th}(X/X_0)$ better captures the initial linear behaviour (for large values of X/X_0) as well as the significant increase of the volume reduction rate for larger time scales (small X/X_0 values). Although both functions G^{4th} and G^{2nd} approximate well the global behaviour ($R^2 = 0.9811$ for G^{2nd} and $R^2 = 0.9887$ for G^{4th}), the two different approximations lead to very different experimental shrinkage functions $\alpha_X(X/X_0) = G'(X/X_0)/\phi_0$ as shown in Figure 2.

We adopt the G^{2nd} quadratic function for applying the fully analytical approach and the more accurate fourth-order function G^{4th} for the shortcut numerical approach. The final goal is to estimate with both approaches the effective water diffusion coefficient D and its dependence on temperature T and to compare the results.

It should be observed that there is no physical difference between the shrinkage function $\alpha(\psi)$ obtained with the fully analytical approach and that obtained from the shortcut approach. The two approaches furnish different approximations of the shrinkage function $\alpha(\psi)$ that is an intrinsic property, a sort of fingerprint, of the material under investigation.

In point of fact, during dehydration, the material exhibits structural changes. As a consequence, sample volume can be reduced by an amount that can be greater, less, or equal to the volume of released water. The introduction of the shrinkage function $\alpha(\psi)$ allows us to take this feature into account because α represents the proportionality factor between the pointwise shrinkage velocity and the local water flux. This proportionality factor changes with the water content in a nonlinear fashion for many materials as can be deduced, in a straightforward way, from the nonlinear behaviour of $G(X/X_0)$ or, better to say, from the nonconstant behaviour of $G'(X/X_0)$.

For a material exhibiting a linear calibration curve $G(X/X_0) = 1 - \phi_0\delta(1 - X/X_0)$, the corresponding shrinkage function is constant $\alpha(\psi) = G'(X/X_0)/\phi_0 = \delta$. If $\delta = 1$, the material exhibits ideal shrinkage because volume reduction equals, at each time instant, the volume of released water.

However, in most cases, $G(X/X_0)$ is a nonlinear function of X/X_0. In the specific case of the chayote, $G(X/X_0)$ is an increasing nonlinear function of X/X_0, better approximated by a fourth-order polynomial if we want to accurately describe its behaviour for small values of X/X_0, that is, on long time scales of the dehydration process. This implies that while sample volume reduction and volume of released water are comparable with each other at short time scales, on the contrary, on longer time scales, when the rescaled moisture content X/X_0 is below 40%, a structural collapse of the sample occurs and the volume reduction is two to three times larger than the volume of release water (Figure 2).

5. Analytical Approach

The analytical approach can be easily applied when the calibration curve $L/L_0 = G(X/X_0)$ is well approximated by

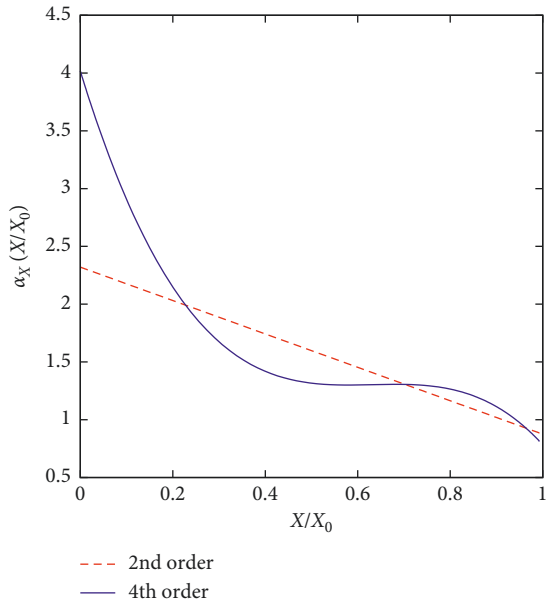

Figure 2: Experimental shrinkage functions $\alpha_X(X/X_0) = G'(X/X_0)/\phi_0$ obtained from $G^{2nd}(X/X_0)$ (equation (15)) and from $G^{4th}(X/X_0)$ (equation (16)).

a linear or a quadratic function because the *first step* is to enforce equation (14) that can be rewritten as

$$\frac{X}{X_0} = \psi_{av}\frac{L}{L_0} = \psi_{av}G\left(\frac{X}{X_0}\right). \tag{17}$$

By solving equation (17) with respect to X/X_0, we obtain an analytic expression for X/X_0 as a function of ψ_{av}.

For a linear G function $G(X/X_0) = 1-\gamma(1-X/X_0)$, equation (17) reads as

$$\frac{X}{X_0} = \psi_{av}\left(1-\gamma\left(1-\frac{X}{X_0}\right)\right), \tag{18}$$

that can be solved with respect to X/X_0, thus obtaining

$$\frac{X}{X_0} = q(\psi_{av}) = \frac{\psi_{av}(1-\gamma)}{1-\psi_{av}\gamma}. \tag{19}$$

Analogously, for a quadratic G function, e.g., equations (15) and (17) read as

$$\frac{X}{X_0} = \psi_{av}\left(1-\gamma_1\left(1-\frac{X}{X_0}\right)-\gamma_2\left(1-\frac{X}{X_0}\right)^2\right), \tag{20}$$

that, solved with respect to X/X_0, gives the following expression for $q(\psi_{av})$:

$$\begin{aligned}\frac{X}{X_0} = q(\psi_{av}) &= \frac{-b+\sqrt{(b^2-4ac)}}{2a},\\ a(\psi_{av}) &= \gamma_2\psi_{av},\\ b(\psi_{av}) &= 1-(\gamma_1+2\gamma_2)\psi_{av},\\ c(\psi_{av}) &= (\gamma_1+\gamma_2-1)\psi_{av}.\end{aligned} \tag{21}$$

In the case of the calibration curve being an n-th order polynomial, then the identification of the $q(\psi_{av})$ function would require the solution of an n-th order equation in X/X_0 and this would be extremely difficult if not analytically impossible.

The *second step* in the analytical approach is to relate ψ_{av} to ψ_P by adopting the following model that has been specifically derived for a one-dimensional drying and shrinkage process (Appendix) and that explicitly takes into account the influence of Bi_m as follows:

$$\psi_{av}(\psi_P; Bi_m) = 1-\frac{\theta(Bi_m)\left((1-\psi_P)/(1-\psi_{eq})\right)^2}{1+\left[\left(\theta(Bi_m)/(1-\psi_{eq})\right)-1-\delta(Bi_m)\right]\left((1-\psi_P)/(1-\psi_{eq})\right)^{1/2}+\delta(Bi_m)\left((1-\psi_P)/(1-\psi_{eq})\right)^2}, \tag{22}$$

$$\theta(Bi_m) = \frac{1-\psi_{eq}}{Bi_m}, \tag{23}$$

$$\delta(Bi_m) = \frac{(1-\psi_{eq})+\theta(Bi_m)(3-2\sigma(Bi_m))}{3(1-\psi_{eq})}, \tag{24}$$

where

$$\sigma(\mathrm{Bi_m}) = \frac{\mathrm{Bi_m}\left(L_{eq}/L_0\right)}{2\lambda_0^2}, \tag{25}$$

$$2\lambda_0 \tan(\lambda_0) - \mathrm{Bi_m}\left(L_{eq}/L_0\right) = 0. \tag{26}$$

The symbol λ_0 represents the smallest positive root of equation (26), and L_{eq}/L_0 is the asymptotic rescaled thickness. The analytic derivation of the equations (22)–(26) relating ψ_{av} to ψ_P and $\mathrm{Bi_m}$ is reported in Appendix and is independent of the shrinkage function $\alpha(\psi)$.

By making use of the analytic expression $X/X_0 = q(\psi_{av})$, equations (19) or (21) (the latter in the case of chayote discoid samples), and the analytical expression for $\psi_{av}(\psi_P; \mathrm{Bi_m})$, equations (22)–(26), the more accurate expression for the shrinkage factor is obtained:

$$\alpha(\psi) = \frac{1}{\phi_0} G'\left(q\left(\psi_{av}(\psi; \mathrm{Bi_m})\right)\right). \tag{27}$$

This can be used to solve the moving boundary model equations (6)–(9).

Figure 3(a) shows the behaviour of $\alpha(\psi)$ obtained with the linear approximation $X/X_0 = \psi_P$, i.e., $\alpha(\psi) = G'(\psi)/\phi_0$ (equation (13), red dashed line) and with the nonlinear model equation (27) (blue curve) for chayote discoid samples with thickness calibration curve $G^{2nd}(X/X_0)$ (equation (15)).

Figure 3(b) shows the corresponding 1-d moving boundary model predictions for L/L_0 vs. X/X_0 and the comparison with experimental data. We observe that the model prediction for L/L_0 vs. X/X_0 with $\alpha(\psi)$ obtained with the linear approximation (red dotted curve) is already satisfactory ($R^2 = 0.935$), but the improvement in model predictions obtained by adopting the nonlinear model equation (27) is significant (blue curve, $R^2 = 0.980$) and leads to a more accurate estimate of water diffusivity.

6. Shortcut Numerical Approach

In Section 5, we have shown that the analytical approach requires two steps in order to evaluate an accurate expression for the $g(\psi_P, \mathrm{Bi_m})$ function, directly relating X/X_0 to ψ_P and $\mathrm{Bi_m}$. The first step is to evaluate the $q(\psi_{av})$ function relating X/X_0 to ψ_{av}. The second step is to evaluate the function $\psi_{av}(\psi_P, \mathrm{Bi_m})$ relating ψ_{av} to ψ_P and $\mathrm{Bi_m}$.

The basic idea behind the shortcut numerical approach is to make a direct use of numerical data obtained with the moving boundary model in order to obtain an accurate expression directly for $X/X_0 = g(\psi_P, \mathrm{Bi_m})$.

The shortcut numerical approach stems from the following observation. In Section 5, we have shown that the shrinkage function $\alpha(\psi) = G'(\psi)/\phi_0$ (equation (13)) obtained with the linear approximation $X/X_0 = \psi_P$ gives reasonably good results in terms of model predictions of experimental data for L/L_0 vs. X/X_0. Figure 4 supports this observation as it shows the good agreement between the experimental thickness calibration data for chayote discoid samples and 1-d moving boundary model predictions (red dotted curve) with $\alpha(\psi)$ given by equation (13) adopting, in this case, the fourth-order more accurate approximating function $G^{4th}(X/X_0)$ (equation (16)).

Therefore, the *first step* in the shortcut approach is the numerical integration of the moving boundary model with the shrinkage function equation (13) obtained with the linear approximation $X/X_0 = \psi_P$ (and with the more accurate $G^{4th}(X/X_0)$ function) in order to obtain a numerical accurate estimate of the $g(\psi_P, \mathrm{Bi_m})$ function, i.e., $X/X_0 = g(\psi_P, \mathrm{Bi_m})$ (Figure 5(a), dots).

The *second step* is to obtain an analytic expression for the $g(\psi_P, \mathrm{Bi_m})$ function by a least-square best fit of numerical data X/X_0 vs. ψ_P by means of the versatile sigmoid function:

$$g(\psi_P, \mathrm{Bi_m}) \simeq S(\psi_P, \mathrm{Bi_m}) = 1 - \frac{\kappa_1 (1-\psi_P)^2}{1 + [\kappa_1 - 1 - \kappa_2](1-\psi_P)^n + \kappa_2 (1-\psi_P)^2}, \tag{28}$$

where κ_1, κ_2, and $n < 2$ are best fit values (Figure 5(a), continuous line).

The more accurate expression for the shrinkage function $\alpha(\psi)$ reads as

$$\alpha(\psi) = \alpha_X(S(\psi, \mathrm{Bi_m})) = \frac{G'(S(\psi, \mathrm{Bi_m}))}{\phi_0}. \tag{29}$$

Figure 5(b) shows the significant difference between the shrinkage function $\alpha(\psi)$ obtained with the linear approximation $X/X_0 = \psi_P$, i.e., $\alpha(\psi) = G'(\psi)/\phi_0$ (equation (13), red dashed line) and with the nonlinear model equations (28) and (29) (blue curve) for chayote discoid samples with thickness calibration curve $G^{4th}(X/X_0)$ (equation (16)).

Figure 4 shows the corresponding 1-d moving boundary model predictions for L/L_0 vs. X/X_0 and the comparison with experimental data. Like for the fully analytical approach, we observe that the model prediction for L/L_0 vs. X/X_0 with $\alpha(\psi)$ obtained with the linear approximation (red dotted curve) is quite satisfactory but the adoption of the nonlinear more refined model for $\alpha(\psi)$, equations (28) and (29), permits the model to perfectly reproduce the experimental thickness calibration data in the entire range of X/X_0 values.

7. Estimation of Water Diffusivity

All the above analysis is independent of the water diffusivity D as the thickness calibration curve L/L_0 vs. X/X_0 is time independent.

The moving boundary model is a time-dependent model usually written in terms of dimensionless space and time variables. Specifically, the dimensionless time adopted is $\tau = tD/L_0^2$, L_0 being the initial sample thickness, i.e., $L_0 = 6$ mm.

Once the shrinkage factor $\alpha(\psi)$ has been determined, resulting the same for the four temperatures under investigation, since no significant differences have been observed in the thickness calibration curves at the different temperatures, the moving boundary model furnishes a unique time-dependent curve $X/X_0 = f(\tau)$ as well as

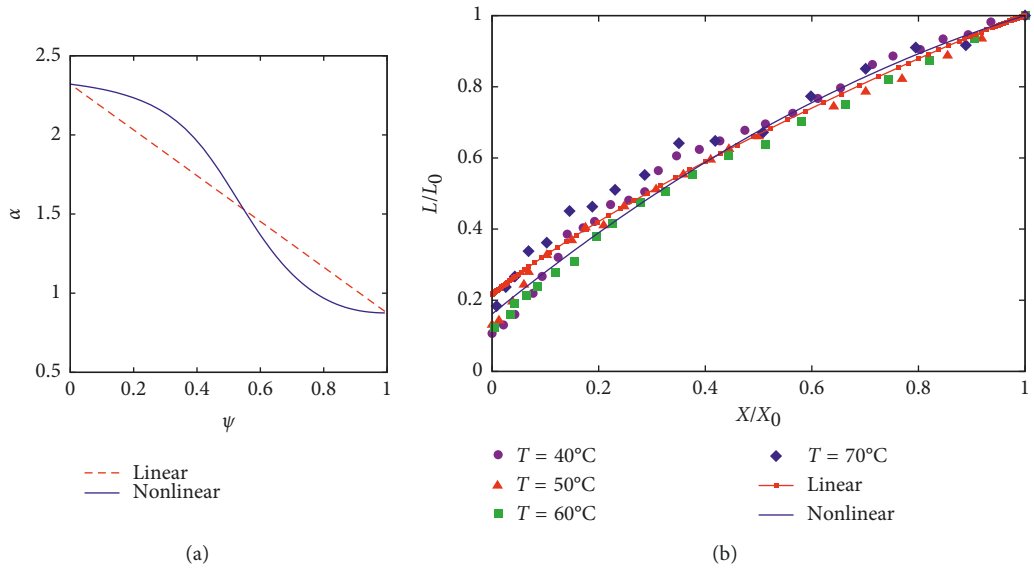

FIGURE 3: (a) $\alpha(\psi)$ obtained with the linear approximation $X/X_0 = \psi_P$, i.e., $\alpha(\psi) = G'(\psi)/\phi_0$ (equation (13)) and with the nonlinear model equation (27) for chayote discoid samples. (b) Comparison between experimental data for L/L_0 vs. X/X_0 for chayote discoid samples and the 1-d moving boundary model predictions obtained with the two different models for $\alpha(\psi)$ shown in (a). For both figures, the thickness calibration curve adopted is $G^{2nd}(X/X_0)$ (equation (15)) and $Bi_m = 2$.

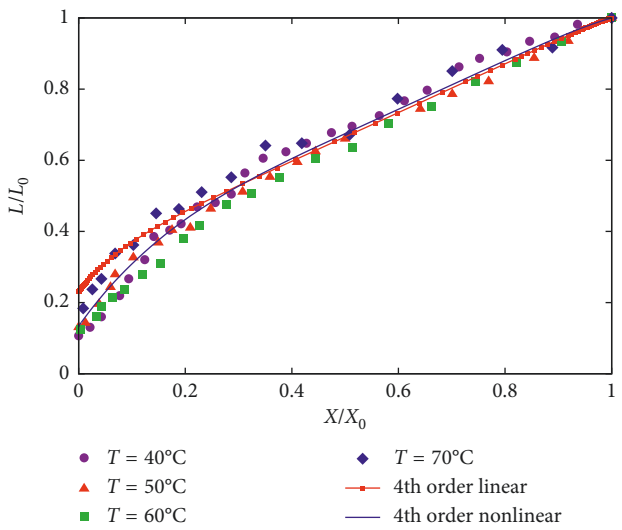

FIGURE 4: Comparison between experimental data for L/L_0 vs. X/X_0 for chayote discoid samples and the 1-d moving boundary model predictions obtained with the two different models for $\alpha(\psi)$ shown in Figure 5(b). The red dotted curve shows model prediction with the α function adopting the linear approximation $X/X_0 = \psi_P$ (equation (13)). The blue curve shows model predictions with the α function adopting the nonlinear approximation equations (28) and (29). The thickness calibration curve adopted is $G^{4th}(X/X_0)$ (equation (16)) and $Bi_m = 2$.

a unique time-dependent curve L/L_0 vs. τ for the four temperatures.

The value of water diffusivity $D(T)$ at each operating temperature is determined by means of a least-square best fit of the model curve $X/X_0 = f(\tau L_0^2/D(T))$ onto the experimental data for time decay of the moisture ratio X/X_0 vs. t at the corresponding temperature T, for the same value of Bi_m, namely, $Bi_m = 2$, adopted for the estimate of the shrinkage function $\alpha(\psi)$.

We followed two different approaches for estimating the shrinkage function $\alpha(\psi)$: the analytical and the shortcut numerical approaches leading to two different expressions for $\alpha(\psi)$, namely, $\alpha^{2nd}(\psi)$ (equation (27)) for the fully analytical approach and $\alpha^{4th}(\psi)$ (equation (29)) for the shortcut numerical approach, and therefore to two different time-dependent curves $X/X_0 = f(\tau)$, $f^{2nd}(\tau)$ and $f^{4th}(\tau)$, respectively.

Figures 6(a) and 6(b) show the comparison between experimental data for X/X_0 vs. (t) (min) for chayote discoid samples and the two model curves.

$f^{2nd}(\tau L_0^2/D^{2nd}(T))$ and $f^{4th}(\tau L_0^2/D^{4th}(T))$ with the best fit diffusivity values are shown in Figure 7. Specifically, from the analytical approach, one obtains $D^{2nd}(40^\circ C) = 6.92 \times 10^{-10}\,(m^2/s)$, $D^{2nd}(50^\circ C) = 9.27 \times 10^{-10}\,(m^2/s)$, $D^{2nd}(60^\circ C) = 1.09 \times 10^{-9}\,(m^2/s)$, and $D^{2nd}(70^\circ C) = 1.35 \times 10^{-9}\,(m^2/s)$, with an Arrhenius correlation function $D(T) = D_0 \exp[-E/(RT)]$ with $D_0^{2nd} = 1.318 \times 10^{-6}\,(m^2/s)$ and $E/R = 2358.38\,(K)$. From the shortcut numerical approach, one obtains $D^{4th}(40^\circ C) = 6.71 \times 10^{-10}\,(m^2/s)$, $D^{4th}(50^\circ C) = 9 \times 10^{-10}\,(m^2/s)$, $D^{4th}(60^\circ C) = 1.06 \times 10^{-9}\,(m^2/s)$, and $D^{4th}(70^\circ C) = 1.31 \times 10^{-9}\,(m^2/s)$ with an Arrhenius correlation function with $D_0^{4th} = 1.28 \times 10^{-6}\,(m^2/s)$ and the same activation energy $E/R = 2358.38\,(K)$.

The agreement between model curves and experimental data for the time decay of the moisture ratio is extremely good for both approaches, and differences between estimated diffusivities are below 3% for all temperatures analyzed.

Diffusivities estimated from both approaches are comparable with literature data for other vegetable products such as carrots $(((2.58 \times 10^{-10})/1.72) \times 10^{-9}\,(m^2/s)$,

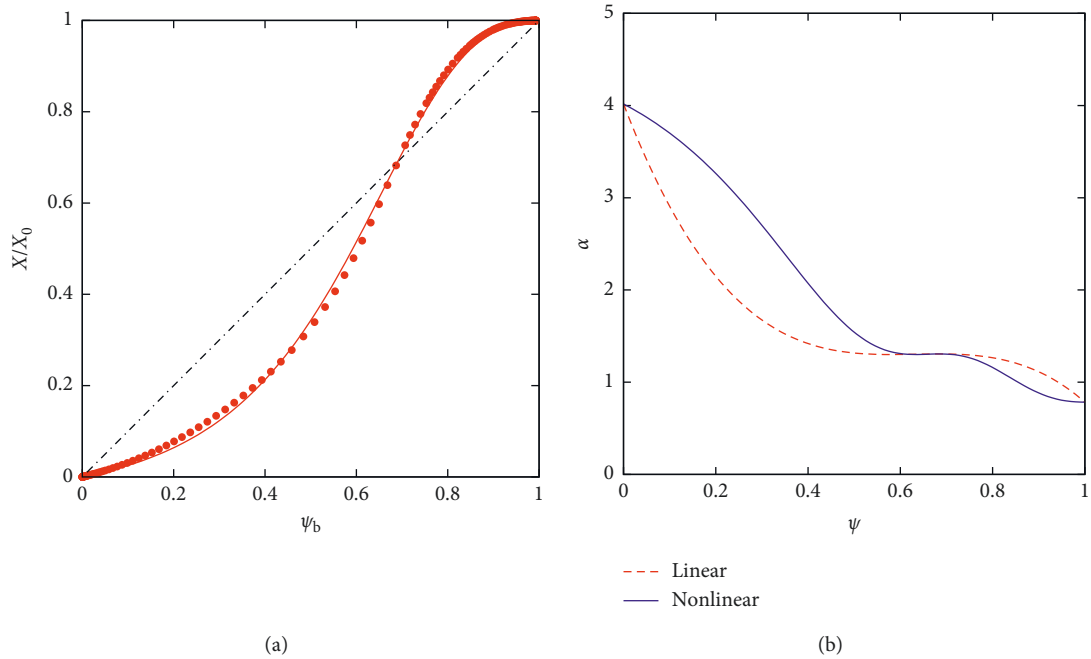

FIGURE 5: (a) X/X_0 vs. ψ_P obtained from the numerical integration of the 1-d moving boundary model with $\alpha(\psi) = G'(\psi)/\phi_0$ and $\mathrm{Bi_m} = 2$. Continuous lines represent the best fit curves $S(\psi_P, \mathrm{Bi_m})$ (equation (28)) with $\kappa_1 = 0.247$, $\kappa_2 = 0.243$, and $n = 0.044$. (b) Shrinkage factor $\alpha(\psi)$ obtained with the linear approximation $X/X_0 = \psi_P$ (equation (13)) and with the nonlinear approximation (equations (28) and (29)). For both figures, $G(X/X_0) = G^{4\mathrm{th}}(X/X_0)$ (equation (16)).

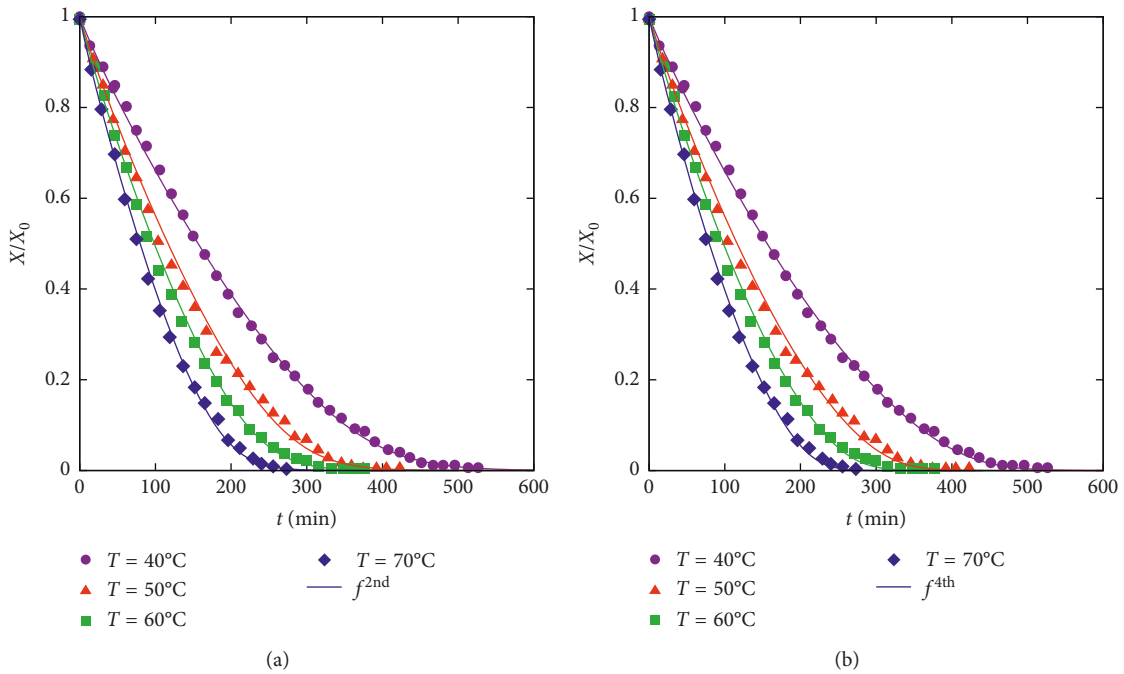

FIGURE 6: Experimental data X/X_0 vs. (t) (min) for chayote discoid samples at four different temperatures $T = 40, 50, 60,$ and 70°C. Least-square best fit with (a) $f^{2\mathrm{nd}}(\tau L_0^2/D^{2\mathrm{nd}}(T))$ from the analytical approach and (b) $f^{4\mathrm{th}}(\tau L_0^2/D^{4\mathrm{th}}(T))$ from the shortcut numerical approach. $L_0 = 6$ mm. $\mathrm{Bi_m} = 2$.

60–90°C), mango ($((2.61 \times 10^{-10})/1.30) \times 10^{-9}$ (m^2/s), 40–70°C), and potatoes ($((3.55 \times 10^{-10})/1.92) \times 10^{-9}$ (m^2/s), 40–85°C) in which shrinkage has also been considered [32–34].

This result confirms that both approaches are robust and reliable and can be indifferently adopted for predicting the time decay of the moisture ratio as well as sample shrinkage during the entire drying process.

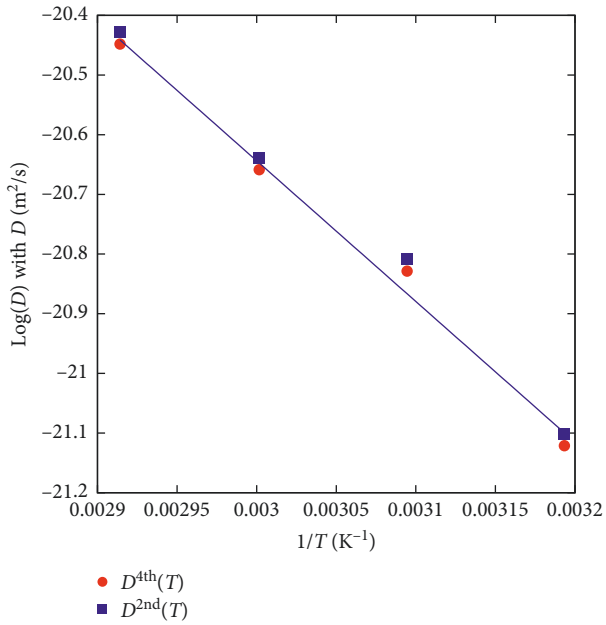

FIGURE 7: Estimated diffusivities $D^{2nd}(T)$ from the analytical approach and $D^{4th}(T)$ from the shortcut numerical approach. Continuous line represents the Arrhenius correlation function $D(T) = D_0 \exp[-E/(RT)]$ with $D_0^{4th} = 1.28 \times 10^{-6}$ (m^2/s) and $E/R = 2358.38$ (K).

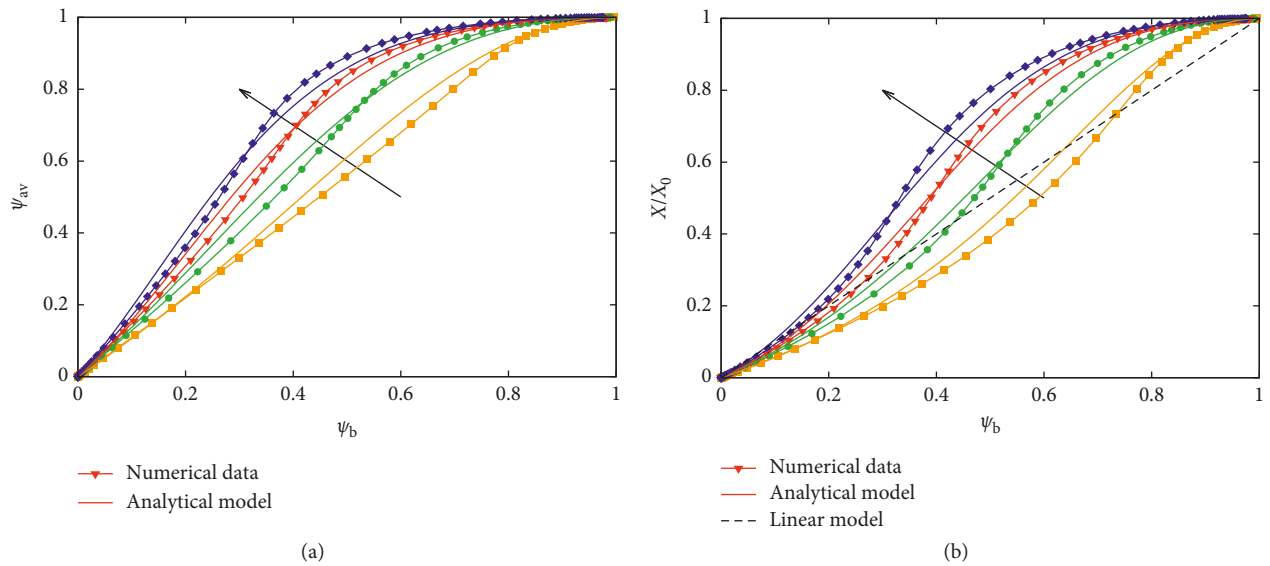

FIGURE 8: Numerical results for ψ_{av} vs. ψ_P (a) and X/X_0 vs. ψ_P (b) for the ideal shrinkage case $\alpha(\psi) = C = 1$, $\phi_0 = 0.5$, and $Bi_m = 1, 3, 5, 7$. Continuous lines represent the nonlinear model predictions (equation (C.1) for ψ_{av} and equations (19) and (C.1) for X/X_0).

8. Conclusions

In this paper, the comparison between the two approaches developed in [21, 22] for mathematical modeling of food drying with shrinkage is carried out.

The developed mathematical model consists of a mass balance equation for water volume fraction evolution, coupled to an equation for the movement of the boundary. The relationship between water concentration and boundary movement is introduced into the system through the dependence of a shrinkage velocity on the concentration gradient times a shrinkage factor α. This represents the constitutive equation of the material.

The two developed approaches (fully analytical and shortcut), precisely dealing with the determination of the shrinkage factor α, were analyzed here and applied to the literature data of chayote discoid sample drying.

We showed that, for the case discussed here, both approaches are able to provide accurate predictions of the experimental data for moisture fraction and thickness reduction, as well as a good estimation of the physical quantities involved (first of all, the water diffusion coefficient) with almost the same computational efforts.

However, this last consideration is true only in this case. The adoption of a one-dimensional simplified model is, in fact, due to conditions of the samples (the symmetrical shape and the value of the aspect ratio) which, as an instance, are in general not found in industrial applications.

For such complex cases, although it is reasonable to assume no differences in terms of prediction capabilities, the computational efforts connected to the fully analytical approach could be very huge compared to the shortcut one or, worst, it could not be pursued at all. Hence, the adoption of the shortcut approach, having demonstrated its efficiency here, can be an attractive opportunity (the only one in the worst cases) to have an accurate description of the evolution of the system through a mathematical model based on balance equations.

Appendix

In this appendix, equations (22)–(26) are derived. Equations (22)–(26) relate ψ_{av} to ψ_P, P being the probe point located at $\zeta_P = \widetilde{L}/2$, $\widetilde{L}(0) = 1$.

The model equations (22)–(26) are derived from the analysis of ψ_{av} vs. ψ_P in the two limiting cases of short and long (asymptotic) time scales and are independent of the shrinkage function $\alpha(\psi)$.

A. Short Time Scales

At the beginning of the process, when the shrinkage is small and therefore negligible, it can be assumed that the water concentration is almost uniform in the inner part of the sample and equal to the initial uniform value $\psi(0) = 1$. Moreover, we can assume that the concentration gradient is localized in a boundary layer of thickness δ close to the boundary where the water volume fraction is ψ_P.

By assuming a linear concentration profile in the boundary layer, the average water concentration in the sample ψ_{av} reads as

$$\psi_{av} = \underbrace{(1-2\delta)}_{\text{inner part}} + 2\underbrace{\left(\delta\frac{1+\psi_P}{2}\right)}_{\text{boundary layer}}. \tag{A.1}$$

The thickness δ of the boundary layer depends on Bi_m and can be estimated by enforcing the linear concentration profile in the boundary layer and the boundary condition:

$$-\left.\frac{\partial\psi}{\partial\zeta}\right|_{\zeta=1/2} = Bi_m\left(\psi_P - \psi_{eq}\right) \longrightarrow \delta = \frac{1-\psi_P}{Bi_m\left(\psi_P - \psi_{eq}\right)}. \tag{A.2}$$

By substituting equation (A.2) for δ into equation (A.1) for ψ_{av}, one obtains an analytic expression for ψ_{av} as a function of ψ_P and Bi_m:

$$\psi_{av} = 1 - \frac{\left(1-\psi_P\right)^2}{Bi_m\left(\psi_P - \psi_{eq}\right)}, \tag{A.3}$$

that is, valid at short time scales, i.e., when $\psi_P \simeq 1$.

By expanding equation (A.2) in power series about the point $\psi_P = 1$, one obtains

$$\psi_{av} = 1 - \frac{\left(1-\psi_P\right)^2}{Bi_m\left(1-\psi_{eq}\right)} + \mathcal{O}\left(1-\psi_P\right)^3, \tag{A.4}$$

and therefore, a quadratic behaviour is predicted for $1-\psi_{av}$ vs. $1-\psi_P$ at the short time scales of the drying process, i.e., for $\psi_P \simeq 1$.

B. Long Time Scales

When approaching the asymptotic behaviour, the sample shrinkage has almost reached its asymptotic value $\widetilde{L}_{eq} = L_{eq}/L_0$ and concentration gradients are very small. Since the shrinkage velocity $\mathbf{v}$ is proportional to the pointwise concentration gradient, its contribution becomes negligible and therefore the water volume fraction profile $\psi(\zeta,\tau)$ can be evaluated by solving the following pure diffusion problem in a 1-d fixed boundary domain $\zeta \in ((-\widetilde{L}_{eq}/2), (\widetilde{L}_{eq}/2))$:

$$\begin{aligned}
&\frac{\partial\widetilde{\psi}}{\partial\tau} = \frac{\partial^2\widetilde{\psi}}{\partial\zeta^2},\\
&\zeta \in \left(\frac{-\widetilde{L}_{eq}}{2}, \frac{\widetilde{L}_{eq}}{2}\right),\\
&\left.\frac{\partial\widetilde{\psi}}{\partial\zeta}\right|_{\zeta=0} = 0,\\
&\left.\frac{\partial\widetilde{\psi}}{\partial\zeta}\right|_{\zeta=\widetilde{L}_{eq}/2} + Bi_m\widetilde{\psi}\Big|_{\zeta=\widetilde{L}_{eq}/2} = 0,
\end{aligned} \tag{B.1}$$

where $\widetilde{\psi} = \psi - \psi_{eq}$ attains the form

$$\widetilde{\psi}(\zeta,\tau) = \sum_{h=0}^{\infty} a_h(\tau)\cos\left(\frac{2\lambda_h\zeta}{\widetilde{L}_{eq}}\right), \tag{B.2}$$

$$a_h(\tau) = a_h(0)\exp\left(-\lambda_h^2\tau\right), \tag{B.3}$$

$$2\lambda_j\tan\left(\lambda_j\right) - Bi_m\widetilde{L}_{eq} = 0, \quad j = 0, 1, \ldots, \infty, \tag{B.4}$$

and the quantities $\widetilde{\psi}_{av}(\tau)$ and $\widetilde{\psi}_P(\tau)$ can be evaluated as

$$\begin{aligned}
&\widetilde{\psi}_{av}(\tau) = \frac{2}{\widetilde{L}_{eq}}\int_0^{\widetilde{L}_{eq}/2}\widetilde{\psi}d\zeta = \sum_{h=0}^{\infty} a_h(\tau)\frac{\sin\lambda_h}{\lambda_h},\\
&\widetilde{\psi}_P(\tau) = \widetilde{\psi}\left(\frac{\widetilde{L}_{eq}}{2},\tau\right) = \sum_{h=0}^{\infty} a_h(\tau)\cos\left(\lambda_k\right).
\end{aligned} \tag{B.5}$$

In the asymptotic limit $\tau \longrightarrow \infty$, given the exponential decay of $a_h(\tau)$, the leading term is the zero-order term $h = 0$ associated with the dominant eigenvalue λ_0, given by the smallest positive root of equation (B.4), so that

$$\lim_{\tau\longrightarrow\infty}\widetilde{\psi}_{\mathrm{av}}(\tau)=a_0(\tau)\frac{\sin(\lambda_0)}{\lambda_0},$$
$$\lim_{\tau\longrightarrow\infty}\widetilde{\psi}_{\mathrm{P}}(\tau)=a_0(\tau)\cos(\lambda_0). \tag{B.6}$$

By merging together equation (B.6), the following relation between $\widetilde{\psi}_{\mathrm{av}}$ and $\widetilde{\psi}_b$ is obtained, valid only for long time scales:

$$\widetilde{\psi}_{\mathrm{av}}=\left(\frac{\tan\lambda_0}{\lambda_0}\right)\widetilde{\psi}_P=\underbrace{\left(\frac{\mathrm{Bi_m}\widetilde{L}_{\mathrm{eq}}}{2\lambda_0^2}\right)}_{\sigma(\mathrm{Bi_m})}\widetilde{\psi}_{\mathrm{P}}. \tag{B.7}$$

Equation (B.7), rewritten in terms of the original variables ψ_{av} and ψ_{P}, reads as

$$\psi_{\mathrm{av}}=\psi_{\mathrm{eq}}+\sigma(\mathrm{Bi_m})\left(\psi_{\mathrm{P}}-\psi_{\mathrm{eq}}\right), \tag{B.8}$$

highlighting a linear relationship between ψ_{av} and $(\psi_{\mathrm{P}}-\psi_{\mathrm{eq}})$ at long time scales of the drying process, i.e., for $\psi_{\mathrm{P}}\simeq\psi_{\mathrm{eq}}$.

C. A Connection between Short and Long Time Scales

In order to have an expression for ψ_{av} vs. ψ_{P} reliable in the whole range $\psi_{\mathrm{P}}\in(\psi_{\mathrm{eq}},1)$, the following sigmoid function is adopted (equation (22) in the main text)

$$\psi_{\mathrm{av}}(\psi_{\mathrm{P}},\mathrm{Bi_m})=1-\frac{\theta(\mathrm{Bi_m})\left((1-\psi_{\mathrm{P}})/(1-\psi_{\mathrm{eq}})\right)^2}{1+\left[\left(\theta(\mathrm{Bi_m})/(1-\psi_{\mathrm{eq}})\right)-1-\delta(\mathrm{Bi_m})\right]\left((1-\psi_{\mathrm{P}})/(1-\psi_{\mathrm{eq}})\right)^{1/2}+\delta(\mathrm{Bi_m})\left((1-\psi_{\mathrm{P}})/(1-\psi_{\mathrm{eq}})\right)^2}, \tag{C.1}$$

that satisfies the two physical constraints $\psi_{\mathrm{av}}(1)=1$ (uniform initial water concentration) and $\psi_{\mathrm{av}}(\psi_{\mathrm{eq}})=\psi_{\mathrm{eq}}$ (uniform water concentration equal to the equilibrium concentration ψ_{eq} in the asymptotic limit).

The two parameters $\theta(\mathrm{Bi_m})$ and $\delta(\mathrm{Bi_m})$ entering equation (C.1) can be obtained by enforcing the two limit behaviours, equation (A.4) for $\psi_{\mathrm{P}}\simeq1$ and equation (B.8) for $\psi_{\mathrm{P}}\simeq\psi_{\mathrm{eq}}$.

By expanding equation (C.1) in power series about the point $\psi_{\mathrm{P}}=1$, one obtains

$$\psi_{\mathrm{av}}=1-\theta(\mathrm{Bi_m})\left(1-\psi_{\mathrm{P}}/1-\psi_{\mathrm{eq}}\right)^2+\mathcal{O}(1-\psi_{\mathrm{P}})^{5/2}. \tag{C.2}$$

By comparing equation (C.2) with equation (A.4) valid when $\psi_{\mathrm{P}}\simeq1$, one obtains for $\theta(\mathrm{Bi_m})$:

$$\theta(\mathrm{Bi_m})=\frac{(1-\psi_{\mathrm{eq}})}{\mathrm{Bi_m}}. \tag{C.3}$$

By expanding equation (C.1) in power series about the point $\psi_{\mathrm{P}}=\psi_{\mathrm{eq}}$, one obtains

$$\psi_{\mathrm{av}}=\psi_{\mathrm{eq}}+\frac{(1-\psi_{\mathrm{eq}})+3\gamma(\mathrm{Bi_m})-3\delta(\mathrm{Bi_m})(1-\psi_{\mathrm{eq}})}{2\gamma(\mathrm{Bi_m})}\cdot\left(\psi_{\mathrm{P}}-\psi_{\mathrm{eq}}\right). \tag{C.4}$$

By comparing equation (C.4) with the asymptotic behaviour equation (B.8), one obtains the following expression for $\delta(\mathrm{Bi_m})$:

$$\delta(\mathrm{Bi_m})=\frac{(1-\psi_{\mathrm{eq}})+\gamma(\mathrm{Bi_m})(3-2\sigma(\mathrm{Bi_m}))}{3(1-\psi_{\mathrm{eq}})}, \tag{C.5}$$

where $\sigma(\mathrm{Bi_m})$ is given by equation (B.7).

It is important to point out that the analytical expression derived above is independent of the shrinkage factor $\alpha(\psi)$ and only the asymptotic rescaled thickness L_{eq}/L_0 enters into equations (C.1), (C.3), and (C.5). Therefore, it can be applied, in principle, to any food material characterized by a dominant one-dimensional shrinkage.

The analytic derivation proposed above is the one-dimensional version of the two-dimensional relation derived in [21] for 2-d square cross sections.

Reliability and accuracy of the analytical expression equations (C.1), (C.3), and (C.5) containing no fitting parameters are confirmed by direct comparison with numerical results for ψ_{av} vs. ψ_{P}, shown in Figure 8(a), obtained in the ideal shrinkage benchmark case $\alpha(\psi)=C=1$, $\phi_0=0.5$, for $\mathrm{Bi_m}=1,3,5,7$. Figure 8(b) shows the good agreement between numerical data for X/X_0 vs. ψ_P and the model predictions in the ideal shrinkage case $C=1$ for which equation (19) holds true with $\gamma=C\phi_0$.

Nomenclature

$\mathrm{Bi_m}$:	Biot number (−), equation (4)
D:	Water diffusion coefficient ($\mathrm{m^2/s}$)
$D^{2\mathrm{nd}}$:	D estimated from $G^{2\mathrm{nd}}$ ($\mathrm{m^2/s}$)
$D^{4\mathrm{th}}$:	D estimated from $G^{4\mathrm{th}}$ ($\mathrm{m^2/s}$)
$g(\psi_{\mathrm{P}},\mathrm{Bi_m})$:	Function relating X/X_0 to ψ_{P} (−), equation (12)
$G(X/X_0)$:	Thickness calibration curve (−), equation (11)
$G^{2\mathrm{nd}}(X/X_0)$:	2nd order polynomial approx. of $G(X/X_0)$ (−), equation (15)
$G^{4\mathrm{th}}(X/X_0)$:	4th order polynomial approx. of $G(X/X_0)$ (−), equation (16)
$\widetilde{L}=L/L_0$:	Dimensionless sample thickness (−)
L_0:	Initial sample thickness (m)
L_{r}:	Reference length (m)
$q(\psi_{\mathrm{av}})$:	Function relating X/X_0 to ψ_{av} (−), equations (19) and (21)
R_0:	Initial sample radius (m)
S:	Dimensionless sample surface (−)
$S(\psi_P,\mathrm{Bi_m})$:	Sigmoidal function (−), equation (28)

T: Operating temperature (K)
$\mathbf{v}$: Dimensionless shrinkage velocity (−), equation (4)
V: Dimensionless sample volume (−).

Greek Symbols

$\alpha(\psi)$: Shrinkage function (−)
α_X: Experimental shrinkage function (−), equation (11)
β_j, γ_j: Polynomial expansion coefficients (−), equations (15)–(16)
∇: Dimensionless gradient operator (−)
$\tau = tD/L_r^2$: Dimensionless time (−)
ϕ: Water volume fraction (−)
ϕ_0: Initial water volume fraction (−)
$\psi = \phi/\phi_0$: Rescaled water volume fraction (−)
ψ_{av}: Average value of ψ (−), equation (14)
ψ_{eq}: ψ at equilibrium (−)
ψ_{P}: ψ at the probe point P (−).

Data Availability

The data used to support the findings of this study are included within the article.

Conflicts of Interest

The authors declare that there are no conflicts of interest regarding the publication of this paper.

References

[1] A. K. Datta, "Porous media approaches to studying simultaneous heat and mass transfer in food processes. i: problem formulations," *Journal of Food Engineering*, vol. 80, no. 1, pp. 80–95, 2007.

[2] M. Giona, A. Brasiello, and S. Crescitelli, "Stochastic foundations of undulatory transport phenomena: generalized Poisson-kac processes—part III extensions and applications to kinetic theory and transport," *Journal of Physics A: Mathematical and Theoretical*, vol. 50, no. 33, 2017.

[3] M. Giona, A. Brasiello, and S. Crescitelli, "Stochastic foundations of undulatory transport phenomena: generalized Poisson-kac processes—part II irreversibility, norms and entropies," *Journal of Physics A: Mathematical and Theoretical*, vol. 50, no. 33, 2017.

[4] A. Brasiello, S. Crescitelli, and M. Giona, "One-dimensional hyperbolic transport: positivity and admissible boundary conditions derived from the wave formulation," *Physica A: Statistical Mechanics and its Applications*, vol. 449, pp. 176–191, 2016.

[5] M. Giona, A. Brasiello, and S. Crescitelli, "Ergodicity-breaking bifurcations and tunneling in hyperbolic transport models," *EPL*, vol. 112, no. 3, 2015.

[6] P. J. Hoogerbrugge and J. M. V. A. Koelman, "Simulating microscopic hydrodynamic phenomena with dissipative particle dynamics," *Europhysics Letters (EPL)*, vol. 19, no. 3, pp. 155–160, 1992.

[7] H. Vu and E. Tsotsas, "Mass and heat transport models for analysis of the drying process in porous media: a review and numerical implementation," *International Journal of Chemical Engineering*, vol. 2018, Article ID 9456418, 13 pages, 2018.

[8] V. R. Sagar and P. Suresh Kumar, "Recent advances in drying and dehydration of fruits and vegetables: a review," *Journal of Food Science and Technology*, vol. 47, no. 1, pp. 15–26, 2010.

[9] L. Bennamoun, L. Fraikin, and A. Léonard, "Modeling and simulation of heat and mass transfer during convective drying of wastewater sludge with introduction of shrinkage phenomena," *Drying Technology*, vol. 32, no. 1, pp. 13–22, 2014.

[10] T. Defraeye, "Advanced computational modelling for drying processes - a review," *Applied Energy*, vol. 131, pp. 323–344, 2014.

[11] A. Brasiello, S. Crescitelli, and G. Milano, "A multiscale approach to triglycerides simulations: from atomistic to coarse-grained models and back," *Faraday Discussions*, vol. 158, pp. 479–492, 2012.

[12] A. Brasiello, L. Russo, C. Siettos, G. Milano, and S. Crescitelli, "Multi-scale modelling and coarse-grained analysis of triglycerides dynamics," *Computer Aided Chemical Engineering*, vol. 28, pp. 625–630, 2010.

[13] A. Brasiello, G. Adiletta, P. Russo, S. Crescitelli, D. Albanese, and M. Di Matteo, "Mathematical modeling of eggplant drying: shrinkage effect," *Journal of Food Engineering*, vol. 114, no. 1, pp. 99–105, 2013.

[14] L. Mayor and A. M. Sereno, "Modelling shrinkage during convective drying of food materials: a review," *Journal of Food Engineering*, vol. 61, no. 3, pp. 373–386, 2004.

[15] F. M. Pacheco-Aguirre, M. A. García-Alvarado, E. Corona-Jiménez, H. Ruiz-Espinosa, O. Cortés-Zavaleta, and I. I. Ruiz-López, "Drying modeling in products undergoing simultaneous size reduction and shape change: appraisal of deformation effect on water diffusivity," *Journal of Food Engineering*, vol. 164, pp. 30–39, 2015.

[16] J. Aprajeeta, R. Gopirajah, and C. Anandharamakrishnan, "Shrinkage and porosity effects on heat and mass transfer during potato drying," *Journal of Food Engineering*, vol. 144, pp. 119–128, 2015.

[17] A. Brasiello, S. Crescitelli, G. Adiletta, M. Di Matteo, and D. Albanese, "Mathematical model with shrinkage of an eggplant drying process," *Chemical Engineering Transactions*, vol. 24, pp. 451–456, 2011.

[18] S. Curcio and M. Aversa, "Influence of shrinkage on convective drying of fresh vegetables: a theoretical model," *Journal of Food Engineering*, vol. 123, pp. 36–49, 2014.

[19] A. Brasiello, G. Iannone, G. Adiletta, S. De Pasquale, P. Russo, and M. Di Matteo, "Mathematical model for dehydration and shrinkage: prediction of eggplant's MRI spatial profiles," *Journal of Food Engineering*, vol. 203, pp. 1–5, 2017.

[20] B. Ortiz-García-Carrasco, E. Yañez-Mota, F. M. Pacheco-Aguirre et al., "Drying of shrinkable food products: appraisal of deformation behavior and moisture diffusivity estimation under isotropic shrinkage," *Journal of Food Engineering*, vol. 144, pp. 138–147, 2015.

[21] A. Adrover, A. Brasiello, and G. Ponso, "A moving boundary model for food isothermal drying and shrinkage: general setting," *Journal of Food Engineering*, vol. 244, pp. 178–191, 2019.

[22] A. Adrover, A. Brasiello, and G. Ponso, "A moving boundary model for food isothermal drying and shrinkage: a shortcut numerical method for estimating the shrinkage factor," *Journal of Food Engineering*, vol. 244, pp. 212–219, 2019.

[23] Y.-O. Tu and A. C. Ouano, "Model for the kinematics of polymer dissolution," *IBM Journal of Research and Development*, vol. 21, no. 2, pp. 131–142, 1977.

[24] J. Papanu, D. Soane (Soong), A. Bell, and D. Hess, "Transport models for swelling and dissolution of thin polymer films," *Journal of Applied Polymer Science*, vol. 38, no. 5, pp. 859–885, 1989.

[25] A. Adrover and M. Nobili, "Release kinetics from oral thin films: theory and experiments," *Chemical Engineering Research and Design*, vol. 98, pp. 188–201, 2015.

[26] A. Adrover, G. Varani, P. Paolicelli et al., "Experimental and modeling study of drug release from hpmc-based erodible oral thin films," *Pharmaceutics*, vol. 10, no. 4, 2018.

[27] I. I. Ruiz-López, H. Ruiz-Espinosa, P. Arellanes-Lozada, M. E. Bárcenas-Pozos, and M. A. García-Alvarado, "Analytical model for variable moisture diffusivity estimation and drying simulation of shrinkable food products," *Journal of Food Engineering*, vol. 108, no. 3, pp. 427–435, 2012.

[28] J. Crank and E. Crank, *The Mathematics of Diffusion*, Oxford Science Publications, Clarendon Press, Oxford, UK, 1979.

[29] J. E. Lozano, E. Rotstein, and M. J. Urbicain, "Shrinkage, porosity and bulk density of foodstuffs at changing moisture contents," *Journal of Food Science*, vol. 48, no. 5, pp. 1497–1502, 1983.

[30] J. Madiouli, J. Sghaier, D. Lecomte, and H. Sammouda, "Determination of porosity change from shrinkage curves during drying of food material," *Food and Bioproducts Processing*, vol. 90, no. 1, pp. 43–51, 2012.

[31] USDA US Department of Agriculture, "Food composition databases," https://ndb.nal.usda.gov/ndb/.

[32] A. O. Dissa, H. Desmorieux, J. Bathiebo, and J. Koulidiati, "Convective drying characteristics of Amelie mango (Mangifera Indica L. cv. "Amelie") with correction for shrinkage," *Journal of Food Engineering*, vol. 88, no. 4, pp. 429–437, 2008.

[33] M. Zielinska and M. Markowski, "Air drying characteristics and moisture diffusivity of carrots," *Chemical Engineering and Processing: Process Intensification*, vol. 49, no. 2, pp. 212–218, 2010.

[34] L. Hassini, S. Azzouz, R. Peczalski, and A. Belghith, "Estimation of potato moisture diffusivity from convective drying kinetics with correction for shrinkage," *Journal of Food Engineering*, vol. 79, no. 1, pp. 47–56, 2007.